

Northumbria Research Link

Citation: Tian, Zhen, Yao, Yicun, Yuan, Jinhui, Zhang, Liqiang, Chen, Nan Kuang, Zhang, Yanqing, Wang, Minghong and Wu, Qiang (2022) Post chemical Etching of Tapered Seven-Core Fiber Sensor for Enhanced Figure of Merit. *Optics Letters*, 47 (18). pp. 4672-4675. ISSN 0146-9592

Published by: OSA

URL: <https://doi.org/10.1364/OL.469107> <<https://doi.org/10.1364/OL.469107>>

This version was downloaded from Northumbria Research Link:
<https://nrl.northumbria.ac.uk/id/eprint/49948/>

Northumbria University has developed Northumbria Research Link (NRL) to enable users to access the University's research output. Copyright © and moral rights for items on NRL are retained by the individual author(s) and/or other copyright owners. Single copies of full items can be reproduced, displayed or performed, and given to third parties in any format or medium for personal research or study, educational, or not-for-profit purposes without prior permission or charge, provided the authors, title and full bibliographic details are given, as well as a hyperlink and/or URL to the original metadata page. The content must not be changed in any way. Full items must not be sold commercially in any format or medium without formal permission of the copyright holder. The full policy is available online: <http://nrl.northumbria.ac.uk/policies.html>

This document may differ from the final, published version of the research and has been made available online in accordance with publisher policies. To read and/or cite from the published version of the research, please visit the publisher's website (a subscription may be required.)



**Northumbria
University**
NEWCASTLE



University Library

Post chemical Etching of Tapered Seven-Core Fiber Sensor for Enhanced Figure of Merit

ZHEN TIAN^{1,2}, YICUN YAO², JINHUI YUAN^{1,3,6}, LIQIANG ZHANG², NAN-KUANG CHEN², YANQING ZHANG², MINGHONG WANG², QIANG WU^{1,4,5,7}

¹*State Key Laboratory of Information Photonics and Optical Communications, Beijing University of Posts and Telecommunications, Beijing 100000, China*

²*School of Physics Sciences and Information Technology, LiaoCheng University, LiaoCheng 252000, China*

³*The Research Center for Convergence Networks and Ubiquitous Services, University of Science & Technology Beijing, Beijing 100083, China.*

⁴*Key Laboratory of Opto-Electronic Information Science and Technology of Jiangxi Province, Nanchang Hangkong University, Nanchang, China*

⁵*Faculty of Engineering and Environment, Northumbria University, Newcastle Upon Tyne NE1 8ST, UK*

⁶ yuanjhui81@163.com

⁷ qiang.wu@northumbria.ac.uk

Received XX Month XXXX; revised XX Month, XXXX; accepted XX Month XXXX; posted XX Month XXXX (Doc. ID 469107); published XX Month XXXX

A post chemical etching process to a tapered seven core fiber (TSCF) is proposed and experimentally demonstrated to effectively adjust the mode profiles of high-order supermodes, aimed to improve the figure of merit (FOM). The experimental results show that the FOM of an etched TSCF (ETSCF) is as high as 1431.36 1/RIU, a 7.32 times enhancement compared to that of TSCF without etching, provided the TSCF has the same taper waist diameter of 19.20 μm . The proposed method opens a new method for optimizing optical fiber sensor performance.

Optical fiber sensors (OFSs) offer a number of advantages compared to the traditional electronic sensors, such as high sensitivity, small size, immunity to electromagnetic interference, remote detection, and resistance against corrosive media [1-3]. OFSs have been extensively applied in the fields of chemistry [4], biomedicine [5] and environmental science [6, 7]. A number of different OFS structures have been proposed, including fiber gratings [8, 9], tapered fibers [10-12], D-etching [13, 14], dislocation fusing [15, 16]. Recently, multicore fiber based supermode fiber interferometer (SFI) has attracted more and more attentions in many sensing applications [17-20]. Several methods have been employed to fabricate the SFI, such as tapering the weakly coupled multicore fiber (the cores are well separated without evanescent field coupling) [21, 22], customizing multicore fiber [23], utilizing home-made multicore fiber [24]. Among these methods, tapering the weakly coupling multicore fiber is the cost-effective method, which could use the commercial multicore fiber as base to customize the SFI structure. After tapering the weakly coupling multicore fiber into smaller diameter, the modes in different cores no longer propagate independently, which will interference with each other and form supermodes[18, 20]. In principle, high-order supermodes would have higher sensitivity if they had a stronger

evanescent field interacting with the surrounding medium. To improve the sensitivity, the general method is to reduce the diameter of the tapered fiber to excite strong evanescent field [20, 25]. However, for traditional tapered multicore fiber, the whole geometry of the tapered cross-section shrinks proportionally with that of non-tapered fiber, where the ratio between the gap of multicores and the taper waist diameter is not controllable. When the gap of multicores and fiber taper waist diameter decreased to a certain value, the fundamental mode coincides with the higher-order mode, and the multicore fiber degenerates into a single-core fiber. This limits the flexible design of OFS structure to improve sensing performance. Chemical etching can reduce the fiber cladding size[26-29], meanwhile maintain the diameter of the fiber core and the gap of multicores [19, 30-32], which makes the design of OFS structure more flexible compared to that of direct tapered sensor. The combination of chemical etching and tapering enables flexible design and improve performance of multicore-based OFS.

In this paper, the performance enhancement of post chemical etching of the tapered seven-core fiber (TSCF) is numerical simulated and experimentally studied. The modal profiles of the supermodes for the TSCF can be adjusted by controlling etching thickness of the cladding, and thus the coupling efficiency between the input field and supermodes and the evanescent interaction with the surrounding medium can also be adjusted. As a result, the figure of merit (FOM) can be improved, along with enhanced extinction ratio (ER) of the transmission dips and refractive index (RI) sensitivity of the sensor. Moreover, the temperature cross sensitivity is kept at the level as low as $\sim 4.56 \times 10^{-6}$ RIU/ $^{\circ}\text{C}$, showing low cross-sensitivity to the temperature.

The seven-core fiber (SCF) used is the commercially available product SM-7C1500 (Fibercore Company), whose cross-section photograph taken by 1000X CCD is shown in Fig. 1(a). As shown in Fig. 1(a), the SCF has a central core (core 4) and six satellite cores (core 1-3, 5-7), where all the cores have identical diameter d of 6.1 μm and core distance r of 35 μm . The SCF is firstly adiabatically

tapered using a commercial combiner manufacturing system (3SAE Technologies, Inc), where the D_1 and L_1 are the diameter and length of the tapered section, and L_2 is the length of the transition zone, as shown in Fig. 1(b). Here, D_1 is chosen as 40 μm , 30 μm , and 25 μm , L_1 and L_2 are chosen as 10 mm and 8 mm, respectively. For the TSCFs of this size have good initial supermode interference [20, 21]. One end of the tapered SCF (TSCF) is spliced with a single mode fiber (SMF), where the central core 4 is acted as the input of the TSCF, and the other end of the TSCF is spliced with a seven-core fiber fanout (fibercore, FAN-7C) as the output of each core. Then the TSCF is immersed in etching solution of 70 °C in a polypropylene (PP) container. During the etching, a super luminescence diode is connected to the input SMF as the launching source, and an optical spectral analyzer (OSA) is applied for recording the transmission spectrum, as shown in Fig. 1(c). The enlarged cross-section of the ETSCF is schematically presented in Fig. 1(d), where D_1 and D_2 are the diameter before and after etching, respectively. And the gray ring with a thickness Δ is the removed layer by chemical etching. It is noted that the length L_1 is mainly controlled by the first step of fiber tapering process due to the fact that the diameter of both taper transition (L_2) and taper waist (L_1) will be reduced synchronously during the etching process.

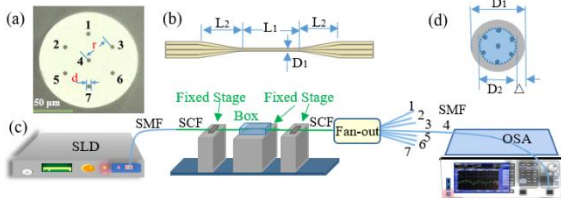


Fig. 1. (a) The photograph of cross-section the seven-core fiber cross-section, (b) schematic diagram of the TSCF, (c) experimental set-up for chemical etching, (d) schematic cross-section of the ETSCF.

When the input light is launched into the central core 4, only the symmetric supermodes are excited, and the interference result of the fundamental mode and second-order supermode [33, 34]. With the finite element method (FEM), the simulated mode profiles of the fundamental mode and second-order supermode of the TSCF are shown in Figs. 2(a) (1) - (8) when the initial diameter of the TSCF D_1 is chosen as 40 μm with different etching thickness Δ . The ERI of each supermode is presented in the bracket above the mode profile.

From Fig. 2 (a), it can be seen that the mode profiles of the fundamental mode and second order supermode can be adjusted by controlling the etching thickness Δ of the TSCF, while the change of the second-order supermode profile is more obvious than that of the fundamental mode. As D_2 decreases, the hot spots are expanded from the satellite core and become connected with each other when D_2 is smaller than 35 μm . On the other side, when D_2 approaches the outside interfaces of the satellite cores the satellite cores are “neglected” in the beam field, as shown in Figs. 2(a) (8), the mode profiles become similar to the cladding mode of an SMF. Because the mode field area of the second-order mode is larger than that of the fundamental mode, and its evanescent field is stronger, it will be more significantly affected by reduction of refractive index due to structural and environmental changes. So its ERI will drop faster than that of the fundamental mode as D_2 changes. The ERI vs. D_2 calculated by the FEM is shown in Fig. 2(b). It can be seen that the ERI of the second-order supermode decreases faster ($\sim 1.29 \times 10^{-3}$ totally reduced) than that of the fundamental one ($\sim 4.47 \times 10^{-4}$

totally reduced) during the etching process, where the Δn_{eff} increases about 2.89 times for the TSCF with D_2 of 25 μm compared to that with D_2 of 40 μm .

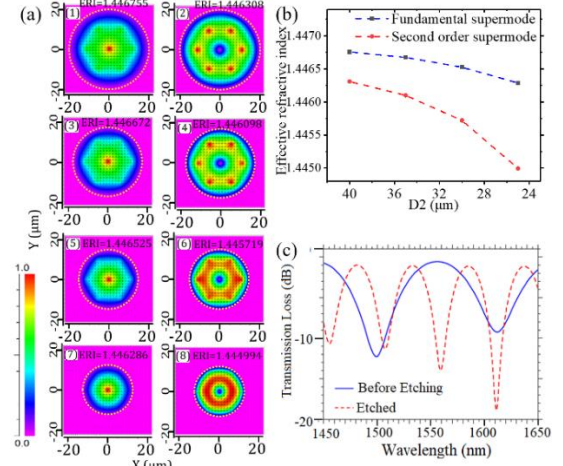


Fig. 2. The mode profiles of the fundamental mode and second-order supermode of the TSCF for (a)(1) - (2) D_2 of 40 μm , (3) - (4) D_2 of 35 μm , (5) - (6) D_2 of 30 μm , and (7) - (8) D_2 of 25 μm , the yellow dotted lines are the fiber outline diagram; (b) The ERI change with D_2 (The change of ERI for each supermode with D_2); (c) Simulated transmission spectra for the TSCF before and after etching with D_2 of 23 μm .

The simulated transmission spectra of the TSCF before ($D_2=40 \mu\text{m}$) and after etching ($D_2=23 \mu\text{m}$) are shown in Fig. 2(c) by the beam propagation method (BPM). The FSR of the transmission is reduced after etching, along with the ER enhancement. The reason may be considered as following. The FSR of the TSCF interferometer can be described as

$$\text{FSR} = \frac{\lambda^2}{L \cdot \Delta n_{\text{eff}}} \quad (1)$$

where L is the length of the coupling section, λ is the free space wavelength, and Δn_{eff} is the ERI difference between the fundamental mode and second-order supermode. As the D_2 decreases from 40 μm to 23 μm , Δn_{eff} increases more than 2.89 times, which induces the reduction of the FSR. The ER enhancement may be due to the change of excitation efficiencies of fundamental and second-order supermodes, when the magnitude ratio of the two modes reaches an optimum value, the ER will be maximum.

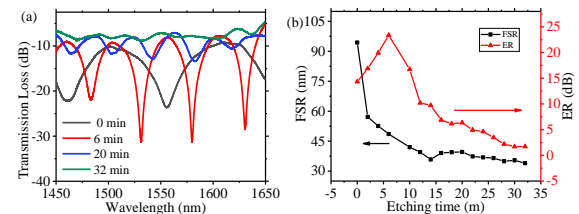


Fig. 3. (a) Transmission spectra of the TSCF with the initial diameter of 40 μm at different etching times, and (b) the relationships between the ER, FSR and the etching time.

The transmission spectra of the TSCF during etching process is shown in Fig. 3(a), and the change of FSR and ER is shown in Fig. 3 (b). In the experiment, the L_1 of the TSCF is 10 mm, and D_1 is 40 μm . The result shows that as etching time increases, the FSR decreases

and in some time slot, the ER has significant enhancement which agrees well with the simulation results. It can be seen from Fig. 3(a) that before etching, the FSR of the interference pattern is 94.66 nm, and the maximum ER is 14.4 dB in the wavelength range of 1450 to 1650 nm. After etching, the ER of the interference spectra reaches the maximum value of 23.5 dB for the etching time of 6 min, as shown in Fig. 3(b). **The reason of the change is shown in the previous paragraph.** However, when etching time is longer than 6 min, the ER decreased significantly. The main reason for the decreasing of ER may be attributed to the non-balanced power distribution between the fundamental mode and the second-order supermode as the satellite cores are exposed to the outer interface.

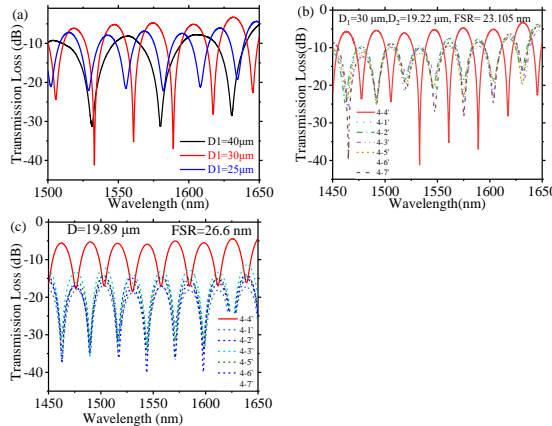


Fig.4. The measured transmission spectra of the TSCF (a) with the maximum ER in the etching process for TSCF with different D_1 ; (b) etched with D_1 of 30 μm and D_2 of 19.22 μm ; (c) with D_1 of 19.89 μm without etching.

The evolution of ER and FSR was found to be similar for TSCFs with different initial diameters D_1 during etching. The optimized transmission spectra of the TSCF with D_1 of 25, 30, and 40 μm are shown in Fig. 4(a). The maximum ER of 35.962 dB and corresponding FWHM 0.32 nm is achieved for the TSCF with D_1 of 30 μm , and the optimized D_2 is 19.22 μm , in this case, the cladding thickness left is theoretically 1 micron. To investigate the difference of transmission spectrum between central core mode and side core mode, transmission spectra lead from the central core and the other six satellite cores of the etched TSCF are recorded using a fan-out. Fig. 4(b) shows the measured transmission spectra of an ETSCF with D_1 of 30 μm and D_2 of 19.22 μm (set as sample A) respectively. For comparison, the transmission spectra of another TSCF which is directly tapered to be with D_1 of 19.89 μm without etching is presented in Fig. 4(c). From Fig. 4(b) and (c), it can be seen that the central core mode (red solid line) and the side core modes (dashed lines) can be oscillated periodically with a phase difference of $\pi/2$, which agrees with the results of other coupled-seven core fiber proved by theory [34] and simulation [35]. It is noted that the magnitude of the center core mode of the etched fiber is slightly higher than that of the side core mode, while in fiber tapered only, the magnitude of the center core mode is significantly larger than that of the side core mode. This is because the etched fiber has relatively larger core diameters (for all seven cores) than that of tapered fiber, which has higher capability to confine light within the side fiber core, resulting in higher magnitude as observed in Fig. 4(b) compared to that of Fig. 4(c).

The RI sensing performances of the ETSCF are also studied. In the experiment, a TSCF with D_1 of 30 μm is chosen, the TSCF was

etched to D_2 of 25.6 μm and then to 19.24 μm (set as sample B). For RI sensing, the TSCF is placed in a PP cell with a dimension of 65×45×15 mm through a pair of pinholes on both sides of the cell for the fiber to pass through. A mixture of glycerol and distilled water in different proportions was used for the test, and the RI of the mixture is calibrated by an Abbe refractometer (NAR-3T ATAGO).

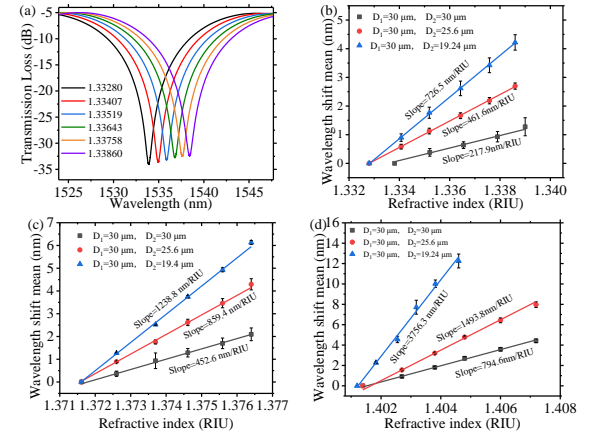


Fig. 5. The transmission curves of the ETSCF with D_1 of 30 μm and D_2 of 19.24 μm when the RI of the solutions varies near the range of (a) 1.33; The RI sensitivity of the TSCF with D_1 of 30 μm at different D_2 near the RI range of (b) 1.33, (c) 1.37, and (d) 1.40. Black, red, and blue curves are the linear fit of dip wavelength shift for the D_2 of 30, 25.6, and 19.24 μm , respectively.

Three different RI ranges are chosen for testing. The transmission spectra of the TSCF with D_1 of 30 μm and D_2 of 19.24 μm are shown in Figs. 5(a). The transmission curves experience red-shift with the increase of RI for all cases. **The mean RI sensitivity is estimated to be 726.5, 1238.8, and 3756.3 nm/RIU in the RI ranges of 1.33, 1.37, and 1.40 respectively, shown as the blue linear fit curve in Fig. 5(b)-(d).** It can be seen that higher sensitivity can be obtained when the surrounding RI increases, which is due to the increased amount of the evanescent wave exposed to the surrounding medium in higher SRI [20].

The effect of D_2 due to the chemical etching on RI sensitivity was also studied, as shown in Fig. 5(b)-(d), by choosing the TSCF with initial taper waist diameter D_1 of 30 μm . As can be seen, the RI sensitivity was improved dramatically with the decrease of D_2 . **The sensitivity enhancement of ETSCF with D_2 about 19.2 μm is estimated to be 333.4%, 273.7% and 472.7% compared to that without etching, at the RI range of 1.33, 1.37 and 1.40 respectively.** The reason is that when the diameter decreases, the increase of the evanescent field in the second-order supermode will be larger than that in the fundamental mode. The RI sensitivity of SCFs directly tapered to 19.89 μm was also investigated experimentally. The transmission spectra of the TSCF with D_1 of 19.89 μm and L_1 of 10 mm are shown in Fig. 6 (a) and Fig. 6 (b). **Its mean RI sensitivity is 657.2 nm/RIU, slightly less than that (726.5 nm/RIU) of the ETSCF with D_2 of 19.20 μm .**

FOM is an important parameter of a sensor, indicated as [36]

$$\text{FOM} = \frac{S}{\text{FWHM}} \quad (2)$$

where FWHM is the full width at half-maximum of the spectrum dip, and S indicates sensitivity. The FOM of the TSCF with D_1 of 19.89 μm (without etching, shown as Fig. 6 (a)) is 195.57 1/RIU,

and the FOM of the ETSCF with D_2 of 19.24 μm (etched from 30 μm to 19.24 μm , shown as in Fig.5 (a)) is 1431.36 1/RIU respectively. The result shows that the FOM of the ETSCF is 7.32 times enhancement than that without etching. This is possibly because that during the etching process, the diameter of fiber sensor decreases gradually, and the modes within the SCF change accordingly. When the magnitude ratio of supermodes and fundamental mode reaches an optimum value, the FWHM can be minimum, which can be monitored in real time.

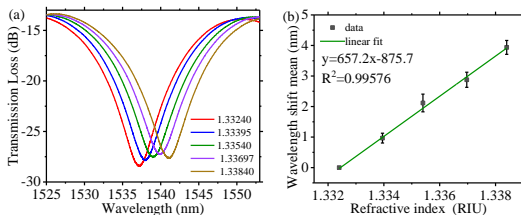


Fig. 6. (a)The transmission curves of the TSCF with D_1 of 19.89 μm ; (b) The RI sensitivity near the RI range of 1.33.

The temperature response of the ETSCF is also studied using another ETSCF (set as sample C) with D_1 of 30 μm and D_2 of 25.2 μm , as shown in Fig. 7. It is shown that a temperature sensitivity of 17.13 pm/ $^{\circ}\text{C}$ has been achieved. The coefficient of determination R^2 of linear fitting is about 0.98672, indicating that the wavelength shift having good linearity. The temperature cross sensitivity for the RI measurement around index RI range of 1.40 is estimated to be as low as 4.56×10^{-6} RIU/ $^{\circ}\text{C}$, which is small enough to allow the ETSCF to operate in a very stable manner.

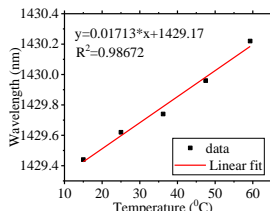


Fig. 7. Position of transmission dip with relationship of temperature

In summary, the effect of post chemical etching of a TSCF is studied. It is found that the post etching is effective for adjusting the mode profiles and the corresponding ERIs of supermodes, especially for higher order supermodes. As a result, the relative strength between different supermodes can be controlled by properly choosing the etching condition to optimize FWHM and thus measurement accuracy. With the almost same taper waist diameter of 19.89 μm , the FOM of the ETSCF ($D_1=30 \mu\text{m}$) is 7.32 times than that of TSCF without etching. The post etching method is a simple and effective technique for adjustment and optimization of the spectral characteristics of a tapered optical fiber interferometer (no core, multi-core, or multimode), which has potential application in the design of tapered optical fiber sensors and communication devices.

Funding. This work was supported in part by the National Natural Science Foundation of China (NSFC) (61875247, 62175097, 62065013), Natural Science Foundation of Shandong Province, China (ZR2020QF086) and by Liaocheng University under Grants (31805180101, 319190301).

References

- Q. Wu, Y. Qu, J. Liu, J. Yuan, S.P. Wan, T. Wu, X.D. He, B. Liu, D. Liu, Y. Ma, Y. Semenova, P. Wang, X. Xin, G. Farrell, *IEEE Sensors Journal*. **21**, 12734(2021).
- M.S. Soares, M. Vidal, N.F. Santos, F.M. Costa, C. Marques, S.O. Pereira, C. Leitao, *Biosensors (Basel)*. **11**, (2021).
- Y. Zhao, J. Zhao, Q.J.S. Zhao, *Sens. Actuator A Phys.* **313**, 112160(2020).
- X. Lu, P.J. Thomas, J.O. Hellevang, *Sensors (Basel)*. **19**, (2019).
- T. Guo, *J. Lightwave Technol.* **35**, 3323(2017).
- Q. Wu, Y. Semenova, P. Wang, G. Farrell, *Opt. Express*. **19**, 7937(2011).
- Y. Bao, Y. Huang, M.S. Hoehler, G. Chen, *Sensors (Basel)*. **19**, (2019).
- F. Chiavaioli, F. Baldini, S. Tombelli, C. Trono, A. Giannetti, *Nanophotonics*. **6**, 663(2017).
- M. Loyez, M. Lobry, R. Wattiez, C. Caucheteur, *Sensors (Basel)*. **19**, (2019).
10. R. Kumar, Y. Leng, B. Liu, J. Zhou, L. Shao, J. Yuan, X. Fan, S. Wan, T. Wu, J. Liu, R. Binns, Y.Q. Fu, W.P. Ng, G. Farrell, Y. Semenova, H. Xu, Y. Xiong, X. He, Q. Wu, *Biosens Bioelectron*. **145**, 111563(2019).
11. P. Xiao, Z. Sun, Y. Huang, W. Lin, Y. Ge, R. Xiao, K. Li, Z. Li, H. Lu, M. Yang, L. Liang, L.P. Sun, Y. Ran, J. Li, B.O. Guan, *Opt Express*. **28**, 15783(2020).
12. M. Arjmand, H. Saghafifar, M. Alijanianzadeh, M. Soltanolkotabi, *Sens. Actuators B Chem.* **249**, 523(2017).
13. F. De-Jun, Z. Mao-Sen, G. Liu, L. Xi-Lu, J. Dong-Fang, *IEEE Sens. J.* **14**, 1673(2014).
14. S. Weng, L. Pei, C. Liu, J. Wang, J. Li, T. Ning, *IEEE PHOTONIC TECH L.* **28**, 1916(2016).
15. Y. Wang, R. Gao, X. Xin, *Opt Express*. **29**, 19703(2021).
16. J. Zhang, W. Zhang, J. Wang, S. Huang, M. Liu, J. Li, L. Wang, *MICROW OPT TECHN LET.* **57**, 709(2015).
17. G. Salceda-Delgado, A. Van Newkirk, J.E. Antonio-Lopez, A. Martinez-Rios, A. Schulgen, R. Amezcu Correa, *Opt. Lett.* **40**, 1468(2015).
18. M.S. Yoon, S.B. Lee, Y.G. Han, *Opt Express*. **23**, 18316(2015).
19. D.A. May-Arrioja, J.R. Guzman-Sepulveda, *J. Lightwave Technol.* **35**, 2695(2017).
20. Z.A.A. Al-Mashhadani, I. Navruz, *OPT FIBER TECHNOL.* **48**, 76(2019).
21. D. Yan, Z. Tian, N.K. Chen, L. Zhang, Y. Yao, Y. Xie, P.P. Shum, K.T.V. Grattan, D. Wang, *Opt Express*. **29**, 9532(2021).
22. G. Zhu, Y. Wang, Z. Wang, R. Singh, C. Marques, Q. Wu, B.K. Kaushik, R. Jha, B. Zhang, S. Kumar, *IEEE Trans. Instrum. Meas.* **71**, 1(2022).
23. J.E. Antonio-Lopez, Z.S. Eznaveh, P. LiKamWa, A. Schulgen, R. Amezcu Correa, *Opt. Lett.* **39**, 4309(2014).
24. L. Chen, Y.-K. Leng, B. Liu, J. Liu, S.-P. Wan, T. Wu, J. Yuan, L. Shao, G. Gu, Y.Q. Fu, H. Xu, Y. Xiong, X.-D. He, Q. Wu, *Sens. Actuators B Chem.* **320**, (2020).
25. H.H.L. Wen Bin Ji, Swee Chuan Tjin, Kin Kee Chow, and Anthony Lim, *IEEE PHOTONIC TECH L.* **24**, (2012).
26. M. Li, R. Singh, C. Marques, B. Zhang, S. Kumar, *Opt Express*. **29**, 38150(2021).
27. G. Son, R.A. Pradono, J. Choi, Y. Jeong, D.S. Han, M. Syahadi, Y. Jung, K. Kwon, H. Bae, K. Yu, *J. Lightwave Technol.* **40**, 4832(2022).
28. S. Kumar, Z. Guo, R. Singh, Q. Wang, B. Zhang, S. Cheng, F.-Z. Liu, C. Marques, B.K. Kaushik, R. Jha, *J. Lightwave Technol.* **39**, 4069(2021).
29. R. Singh, S. Kumar, F.Z. Liu, C. Shuang, B. Zhang, R. Jha, B.K. Kaushik, *Biosens Bioelectron*. **168**, 112557(2020).
30. Y. Cardona-Maya, I. Del Villar, A.B. Socorro, J.M. Corres, I.R. Matias, J.F. Botero-Cadavid, *J. Lightwave Technol.* **35**, 3743(2017).
31. B. Yun, N. Chen, Y. Cui, *IEEE PHOTONIC TECH L.* **19**, 1747(2007).
32. P.I. Kuznetsov, D.P. Sudas, E.A. Savel'ev, *Instrum. Exp. Tech.* **63**, 516(2020).
33. C. Jollivet, A. Mafi, D. Flamm, M. Duparre, K. Schuster, S. Grimm, A. Schulgen, *Opt Express*. **22**, 30377(2014).
34. F.Y.M. Chan, A.P.T. Lau, H.-Y. Tam, *Opt. Express*. **20**, 4548(2012).
35. L. Zhang, Z. Tian, N.-K. Chen, H. Han, C.-N. Liu, K.T.V. Grattan, B.M.A. Rahman, H. Zhou, S.-K. Liaw, C. Bai, *J. Lightwave Technol.* **38**, 1966(2020).
36. Z. Zhu, L. Liu, Z. Liu, Y. Zhang, Y. Zhang, *Opt. Lett.* **42**, 2948(2017).